RESEARCH ARTICLE

Detrital apatite Lu–Hf and U–Pb geochronology applied to the southwestern Siberian margin

Stijn Glorie[1] | Jack Gillespie[1,2] | Alexander Simpson[1] | Sarah Gilbert[3] |
Andrei Khudoley[4] | Nadezhda Priyatkina[5,6] | Martin Hand[1] |
Christopher L. Kirkland[2]

[1]Department of Earth Sciences, University of Adelaide, Adelaide, South Australia, Australia

[2]The Institute for Geoscience Research, School of Earth and Planetary Sciences, Curtin University, Perth, Western Australia, Australia

[3]Adelaide Microscopy, University of Adelaide, Adelaide, South Australia, Australia

[4]Institute of Earth Sciences, St. Petersburg State University, St. Petersburg, Russia

[5]Institute of Precambrian Geology and Geochronology of the Russian Academy of Sciences, St. Petersburg, Russia

[6]New South Wales Institute of Frontiers Geoscience, University of Newcastle, Newcastle, New South Wales, Australia

Correspondence
Stijn Glorie, Department of Earth Sciences, University of Adelaide, Adelaide, SA 5005, Australia.
Email: stijn.glorie@adelaide.edu.au

Funding information
Australian Research Council

Abstract

Apatite is increasingly used in sedimentary provenance studies. However, detrital apatite U–Pb geochronology can be challenging due to the presence of non-radiogenic Pb, its intermediate closure temperature (~350–550°C) and/or age-resetting by metamorphic/metasomatic processes. The Lu–Hf system in apatite has a higher closure temperature (~675–750°C) and is, therefore, more robust to thermal resetting. Here we present the first detrital apatite Lu–Hf age spectra. We have developed a laser-ablation Lu–Hf dating technique, using reaction-cell mass spectrometry, that allows rapid cost-effective analysis, required for detrital apatite studies. The method is best suited to Precambrian detritus, permitting greater radiogenic Hf ingrowth. Using samples from Siberia, we demonstrate: (1) excellent correlations between U–Pb and Lu–Hf dates for apatites from igneous protoliths; and (2) that Lu–Hf dating can detect primary age information in metamorphic grains. Hence, when used in tandem with U–Pb zircon and apatite geochronology, Lu–Hf apatite dating provides a powerful new tool for provenance studies.

1 | INTRODUCTION

Sediment provenance studies commonly use zircons, which are generally robust to weathering and U–Pb isotopic open system behaviour (e.g. Cawood et al., 2012; Fedo et al., 2003). However, more recently other mineral phases such as titanite, rutile and apatite have been used to ascertain provenance, as they can record complementary information to zircon concerning the tectonic history of the hinterland (e.g.

Chew et al., 2020). The use of apatite grains in provenance studies can be particularly powerful as apatites form in a broad compositional range of source lithologies that are otherwise difficult to access. In contrast to zircon, apatite commonly crystallizes in less fractionated magmas (lower SiO_2 concentrations) and, therefore, allows the contribution of mafic rocks to the detrital record to be evaluated (e.g. Gillespie et al., 2018; Jennings et al., 2011). Furthermore, apatites are more susceptible to metamorphic/metasomatic processes compared to zircons (e.g. Harlov, 2015), allowing such processes to be detected.

Modern provenance studies use U–Pb geochronology combined with trace element geochemistry to fingerprint detrital crystals. Metamorphic and metasomatic apatites can readily be recognized based on low concentrations of, for example, Th, Y and light rare earth elements (LREEs) (Glorie et al., 2019; Henrichs et al., 2018, 2019). Apatite in mafic rocks is commonly characterized by high Sr concentrations (Belousova et al., 2002; Jennings et al., 2011). Furthermore, multi-element discrimination plots are now available to categorize the protolith rock type of detrital apatites using their trace element geochemistry (O'Sullivan et al., 2018, 2020).

However, detrital apatite U–Pb geochronology is often challenging, for the following reasons: (1) Apatite commonly incorporates non-radiogenic (initial) Pb, and consequently, detrital apatite dating relies on assumptions about the initial Pb isotopic compositions to calculate single-grain ages (e.g. Chew et al., 2014; Gilbert & Glorie, 2020); (2) U-poor apatites, such as commonly found in low-grade metamorphic rocks (Henrichs et al., 2018, 2019), often remain impossible to date due to the low abundance of radiogenic Pb; (3) When source rocks have been strongly affected by metamorphism or metasomatism, primary apatite crystallization ages are often inaccessible by U–Pb geochronology and thus remains elusive (e.g. Kirkland et al., 2018). Isotopic resetting is particularly common for old detrital apatites, which often record a long history of thermal and/or metasomatic events (e.g. Kirkland et al., 2017).

Here we present a novel approach, involving U–Pb dating in combination with Lu–Hf dating in detrital apatites. The Lu–Hf clock has some advantages over U–Pb dating, which makes it a suitable complementary method for detrital apatite studies: (1) apatite Lu–Hf dating, with a closure temperature of ~675–750°C (Chew & Spikings, 2015), is more robust to thermal resetting and, therefore, apatites may retain a memory of primary crystallization ages in metamorphic (up to upper amphibolite facies) systems (Barfod et al., 2005); (2) given the plausible range of terrestrial initial Hf ratios is small and apatites generally have high $^{176}Lu/^{177}Hf$ ratios (up to 90; Barfod et al., 2003), single-grain ages can be calculated (Simpson et al., 2021). Additionally, given the long half-life (~37 Ga) of the Lu–Hf method (Scherer et al., 2001), the method is best suited to date Precambrian detritus to ensure sufficient radiogenic Hf ingrowth. Hence, when combining detrital Lu–Hf and U–Pb dating, both the magmatic and metamorphic history of source terranes can be evaluated through deep time.

Conventional Lu–Hf dating, involving time-consuming clean-laboratory procedures for individual grains, is realistically not suitable for detrital studies. Here, we present the first laser-ablation-based

This work presents the first detrital apatite Lu–Hf age spectra, using a novel method of laser-ablation reaction-cell mass spectrometry. We demonstrate that the apatite Lu–Hf method retains a memory of primary crystallization ages in metamorphic detritus. We also illustrate that the method can be used to evaluate mafic contributions to sedimentary rocks. Hence, when used in concert with more traditional geochronological techniques (zircon and apatite U–Pb), additional provenance information can be obtained. The new method is quick and cost-effective and has the capability to become a routine tool in future provenance research.

detrital apatite Lu–Hf data using the analytical approach outlined in Simpson et al. (2021). This novel method allows rapid and cost-effective analysis required for detrital apatite studies. We demonstrate the utility of laser-based Lu–Hf dating using a suite of sedimentary samples from the southwestern Siberian margin, which contain apatites from a mixture of felsic, mafic and metamorphic protoliths, spanning the Palaeoproterozoic to early Palaeozoic.

2 | GEOLOGICAL BACKGROUND

The Siberian Craton is composed of an amalgamation of Archean and Palaeoproterozoic high-grade metamorphic basement terranes, intruded by diverse unmetamorphosed Palaeoproterozoic (~1.86–1.87 Ga) post-collisional granites (e.g. Donskaya et al., 2014; Gladkochub et al., 2009; Rosen, 2003; Turkina et al., 2006). The Biryusa Block is one of few locations in Siberia where this ancient basement is exposed from beneath the Mesoproterozoic, Neoproterozoic and Phanerozoic sedimentary rocks that blanket much of the craton (Figure 1).

During the Cryogenian–Ediacaran, the modern southwestern margin of the Siberian Craton probably faced an open ocean, resulting in abundant passive margin sediment deposition in the Biryusa area (Metelkin et al., 2010; Pisarevsky & Natapov, 2003; Romanov et al., 2021). The subsequent progressive closure of the Palaeo-Asian Ocean during the Ediacaran–Devonian induced a prolonged process of island-arc and microcontinents accretions onto the SW Siberian margin, which ultimately formed the Altai–Sayan foldbelt (Buslov et al., 2013; Glorie et al., 2011, 2014). Consequently, Palaeozoic sediments were deposited in the peripheral foreland basin of this orogen, unconformably overlying the Neoproterozoic sedimentary rocks.

3 | STRATIGRAPHY AND SAMPLE DESCRIPTIONS

Samples were taken from the Neoproterozoic–Palaeozoic sedimentary successions in the southwestern peripheral foreland
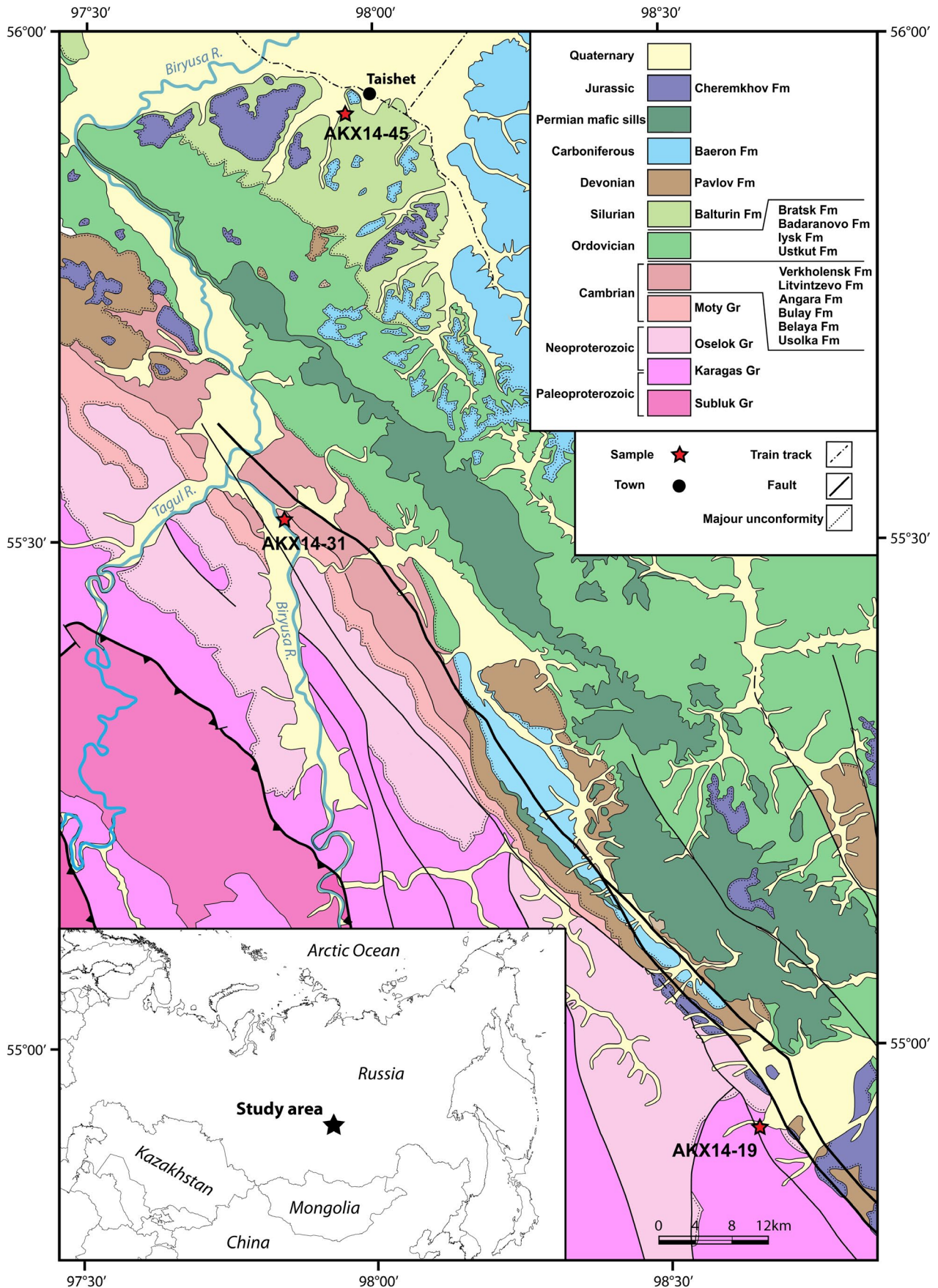
FIGURE 1 Geological map of the study area, the Biryusa uplift at the southwestern margin of the Siberian Craton (after Galimova et al., 2000) with indication of sample locations (star symbols)

basin of the Siberian Craton, near the Biryusa uplift (Figure 1). Sample AKX14-19 (N 54°55′20.8″; E 98°39′24.2″), a subarkosic lithic wacke, was collected from the upper part of the ~3 km thick Neoproterozoic *Karagas Group* (Metelkin et al., 2010). Detrital zircon U–Pb dating of this sample produced an estimate of the maximum depositional age (MDA) for the upper *Karagas Group* of 678 ± 11 Ma, using the youngest single grain criterion (sample PSPC-3 in Priyatkina et al., 2018). The *Karagas Group* is overlain by the ~2.5 km thick Ediacaran *Oselok Group* and the ~150 m thick lower Cambrian *Moty Group* (Kochnev & Karlova, 2010; Letnikova et al., 2013). Sample AKX14-31 (N55°31′20.4″; E 97°50′29.0″), a lithic arenite, was taken from the lower part of the *Moty Group*, which is composed of red, cross-bedded fluvial sandstones with a ~3 m thick basal conglomerate. Detrital zircon U–Pb dating yielded an MDA of 886 ± 6 Ma (*n* = 3; sample PSPC-16 in Priyatkina et al., 2018), which is significantly older than the Cambrian assumed age of deposition. Sample AKX14-45 (N 55°55′20.1″; E 97°57′02.3′), a subarkose to quartz arenite, was taken from the Lower Silurian *Balturin Formation* in the overlaying ~900 m thick Ordovician–Lower Silurian sandstone–siltstone sequence. Detrital zircon U–Pb ages for this sample are presented in File S1 and yield an MDA of 447 ± 4 Ma.

4 | ANALYTICAL METHODS

Apatite grains were liberated using conventional crushing, magnetic and heavy liquid methods. Apatite U–Pb and trace element analysis was conducted simultaneously using a RESOlution 193 nm excimer laser-ablation system, with a 30 μm beam size, coupled to an Agilent 7900 ICP-MS, using identical analytical parameters as in Gillespie et al. (2018). See File S2 for details. Subsequently, apatite crystals that were sufficiently large to allow a second ablation target were analysed for Lu–Hf, in two analytical sessions, using a RESOlution 193 nm excimer laser-ablation system, with a 67 μm beam size, coupled to an Agilent 8900 ICP-MS/MS. See File S2 and Simpson et al. (2021) for analytical conditions. The laser-based Lu–Hf method involves mass-filtering procedures with NH_3 gas in the reaction cell of the mass spectrometer, which allows high-order reaction products $[Hf((NH)(NH_2)(NH_3)_3)^+]$ of ^{176}Hf and ^{178}Hf to be measured free from isobaric interferences at masses 258 and 260 amu respectively. ^{177}Hf is subsequently calculated from ^{178}Hf assuming natural abundances. ^{175}Lu is measured on mass as a proxy for ^{176}Lu (see details in Simpson et al., 2021). Isotope ratios were calculated in LADR (Norris & Danyushevsky, 2018) using NIST 610 as primary standard, and corrected for matrix-induced fractionation (cf. Roberts et al., 2017) using OD306 apatite (1597 ± 7 Ma; Thompson et al., 2016). In-house reference apatites Bamble (corrected Lu–Hf age: 1097 ± 5 Ma) and Harts Range (corrected Lu–Hf age: 343 ± 2 Ma) were monitored for accuracy checks (File S3) and are in excellent agreement with previously published data (Simpson et al., 2021).

$^{176}Hf/^{177}Hf$ ratios are generally high in apatite, allowing $^{176}Lu/^{176}Hf$ ages to be calculated directly for each apatite grain.

The exception is apatite from mafic rocks, which can incorporate significant concentrations of initial Hf during apatite growth. In this study, we applied a common Hf correction to each analysis where ^{177}Hf concentrations were measured above detection limits. The common Hf correction uses the ^{177}Hf concentration to correct for the non-radiogenic component of the ^{176}Hf signal prior to calculating the $^{176}Hf/^{176}Lu$ ratio during data processing in LADR (Simpson et al., 2021). Both corrected and non-corrected ratios are reported in File S4. From our observations, analyses with $^{176}Hf/^{177}Hf$ ratios <0.5 resulted in unreliable common Hf corrections and were, therefore, excluded from interpretations.

5 | RESULTS

The resulting apatite U–Pb dates (File S4) and Lu–Hf dates (File S5) are compared with corresponding zircon U–Pb ages using KDE (kernel density estimate) plots, calculated in IsoplotR (Vermeesch, 2018), in Figure 2. The corresponding trace element data are presented on the multi-element discrimination biplot (Figure 2) from O'Sullivan et al. (2020). Sample AKX14-31 has apatite U–Pb age peaks at ~1.8 Ga and ~0.7 Ga, that are both slightly younger than corresponding zircon age peaks, as well as a range of dates between ~1.2 and 1.7 Ga that are not matched with any zircon dates (Figures 2 and 3). The Sr/Y versus LREE biplot reveals that most of the ~1.7–1.2 Ga apatites are categorized as metamorphic grains based on their trace element composition. The apatite Lu–Hf dates cluster in two age peaks of ~1.8 and ~0.7 Ga, conform with the apatite and zircon U–Pb age peaks, but importantly, without a significant proportion of dates between ~1.7 and ~0.9 Ga. Furthermore, when low LREE apatites (which often suggest low-*T* alteration) are filtered out (blue curve in Figure 2), the apatite Lu–Hf age peaks correlate with the two youngest zircon U–Pb age peaks.

Sample AKX14-19 has similar zircon and apatite U–Pb age peaks compared to sample AKX14-31, with the addition of few ~2.5 and ~3.0 Ga apatite dates and fewer <1 Ga zircon dates. The apatite trace element discrimination plot suggests that the >1.8 Ga apatites were derived from felsic or metamorphic protoliths, while the ~1.5–1.8 and ~0.8 Ga grains plot in the mafic field. The apatites with a mafic origin have a higher contribution of initial Hf (Sr concentrations >500 ppm correspond with $^{176}Hf/^{177}Hf$ ratios <4; File S5) and need significant common Hf corrections, increasing the single-grain age uncertainties for this population and reducing the number of grains for which useful Lu–Hf dates can be determined. However, the resulting apatite Lu–Hf and U–Pb dates are concordant for the mafic apatite population (Figure 3), indicating they are primary ages.

Sample AKX14-45 has generally younger age spectra compared to the other two samples with well-matched zircon and apatite U–Pb age peaks at ~1.7 and ~0.45 Ga. The apatite U–Pb spectrum yields additional dates scattered between ~0.6–1 and ~1.7–1.3 Ga. Based on their trace element composition, the youngest apatites plot mostly near the boundary of the mafic and alkaline fields, while the ~1.6–1.8 Ga grains are categorized as felsic. The other apatite dates have generally lower LREE compositions, suggesting they might reflect a degree of low-*T*

FIGURE 2 (Left) Kernel density estimate (KDE) plots, showing zircon U–Pb age spectra in purple, apatite U–Pb age spectra in green and apatite Lu–Hf age spectra in salmon pink. For samples AKX14-31 and AKX14-45, an extra KDE curve is included (in blue), showing apatite Lu–Hf age spectra excluding datapoints with low (<500 ppm) LREE (=La + Ce + Sm + Nd) concentrations. Rug plots are included for each dataset (in corresponding colours). Each plot was constructed in IsoplotR (Vermeesch, 2018). (right) LREE versus Sr/Y biplot with indication of lithological discrimination fields, following O'Sullivan et al. (2020). The symbols represent the trace element composition for each analysed apatite, colour coded to their U–Pb ages. The abbreviations for each lithological discrimination field are: ALK = alkali-rich igneous rocks; IM = mafic I-type granitoids and mafic igneous rocks; LM = low- and medium-grade metamorphic and metasomatic; HM = partial-melts/leucosomes/high-grade metamorphic; S = S-type granitoids and high aluminium saturation index (ASI) "felsic" I-types; UM = ultramafic rocks including carbonatites, lherzolites and pyroxenites (O'Sullivan et al., 2020)
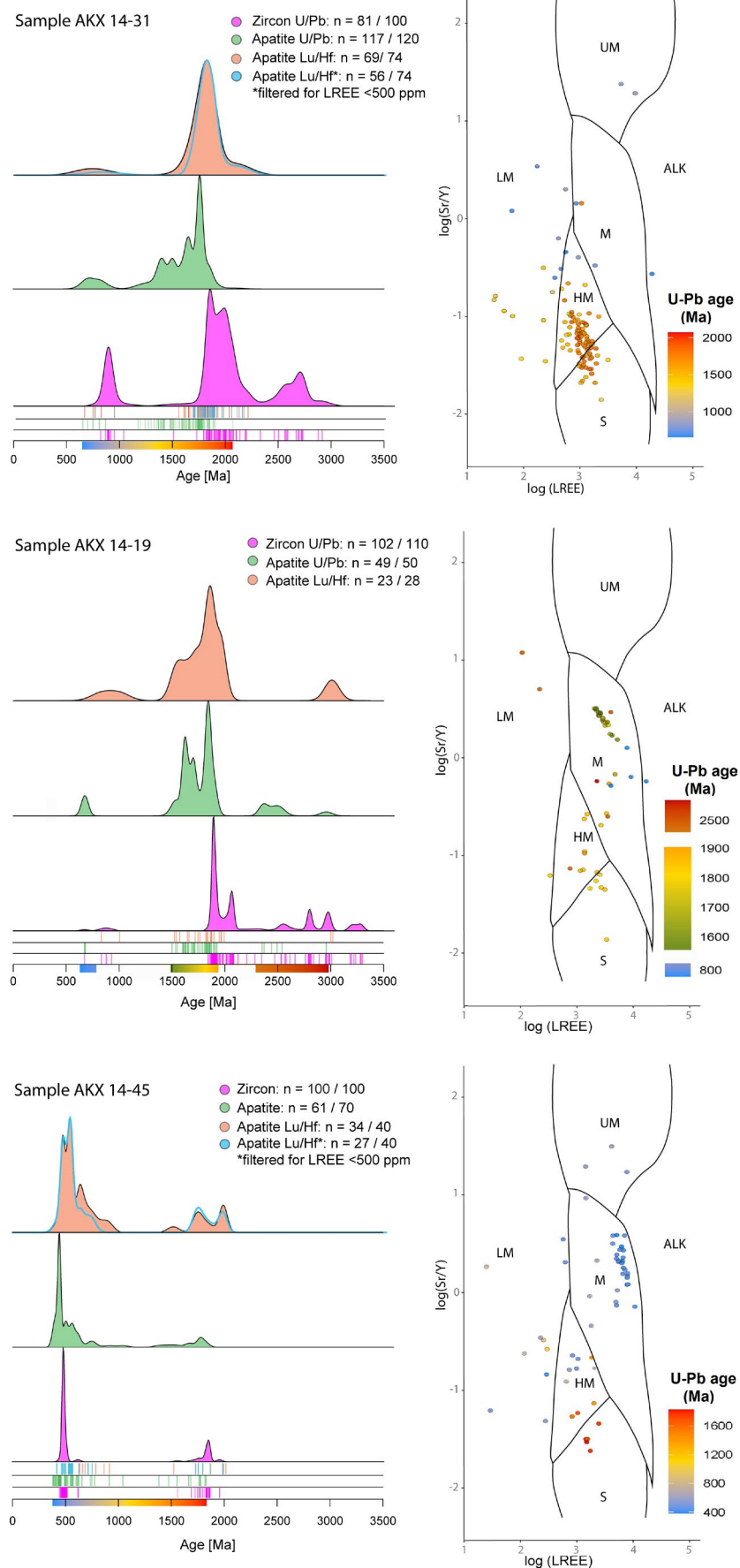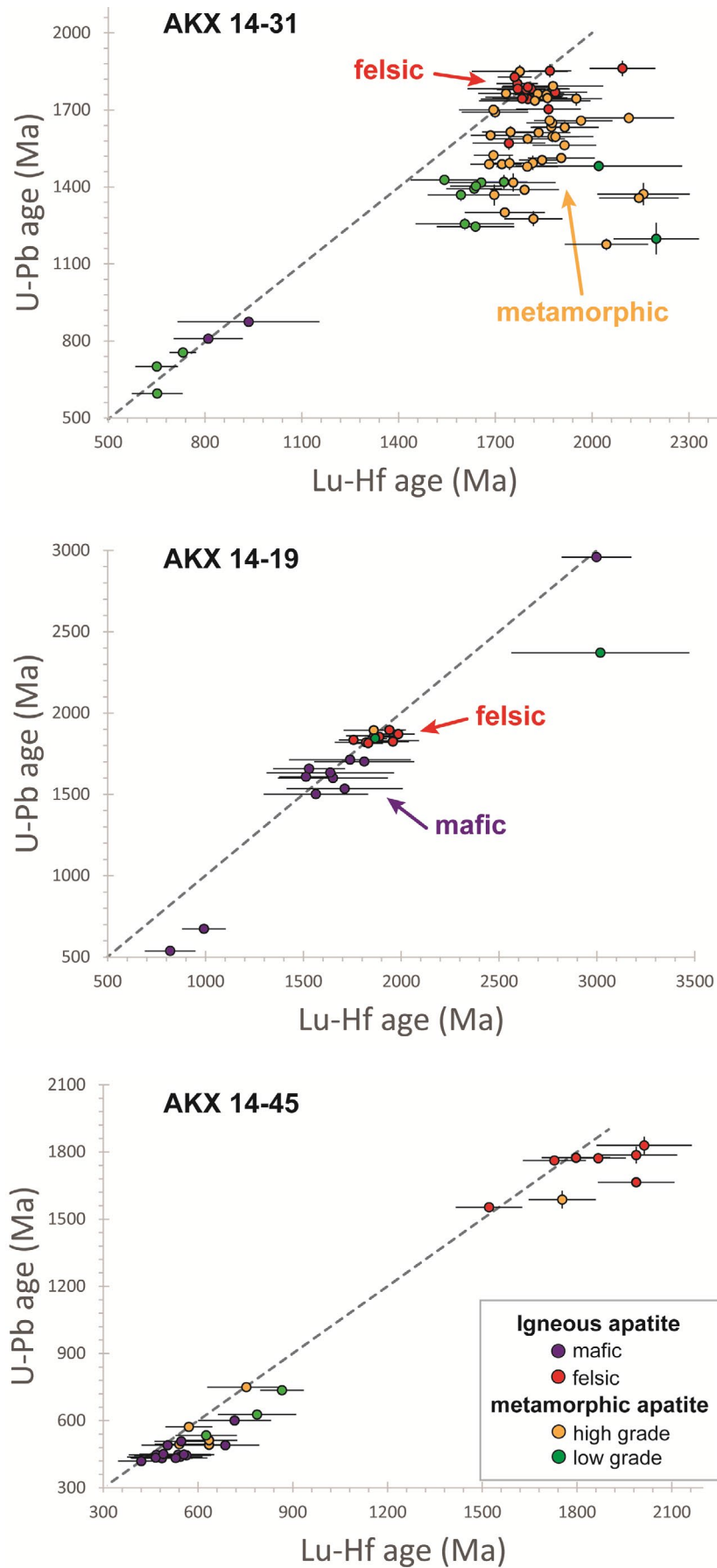
FIGURE 3 Apatite U–Pb versus Lu–Hf age biplot for each individual grain that was double dated. The symbol colours indicate the rock lithologies the apatites were derived from, categorized using the apatite trace element chemistry (Sr/Y ratio and LREE concentrations) and the O'Sullivan et al. (2020) discrimination diagram. The Lu–Hf and U–Pb dates are concordant for the apatites derived from felsic and mafic igneous rocks. For Palaeoproterozoic–Mesoproterozoic metamorphic grains in sample AKX 14–31, the U–Pb system records isotopic open system behaviour, whereas the Lu–Hf system retains primary igneous age information
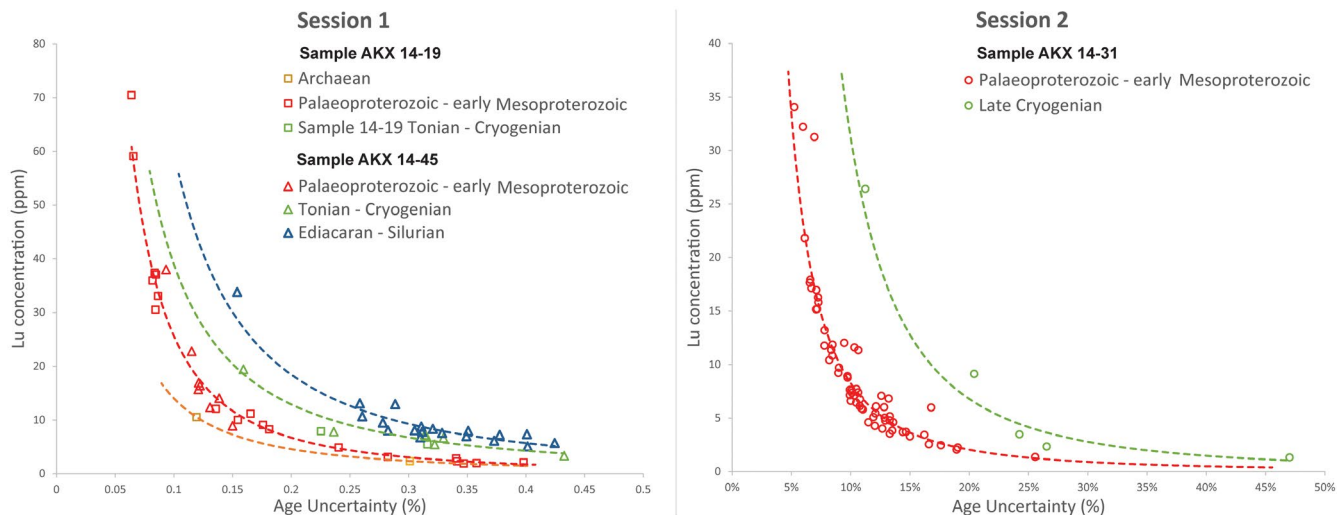
FIGURE 4 Single-grain Lu–Hf age uncertainty (2σ in %) versus Lu concentration (ppm), colour coded to Lu–Hf age. These plots serve as a recipe for anticipated uncertainties in future studies for given Lu concentrations and expected age using a 67 μm laser beam size. The sensitivity increase in session 2 relative to session 1 can be attributed to the addition of N_2 carrier gas in session 2 (see details in method table)

alteration. The Lu–Hf age spectrum matches the apatite U–Pb spectrum, and when grains with LREE <500 ppm are filtered out, the Lu–Hf KDE peaks are tighter and a better match with the zircon age spectrum.

6 | Lu–Hf AGE UNCERTAINTY

The reported uncertainties on the Lu–Hf dates include the signal precision on the calculated ratio, and uncertainties associated with the NIST610 primary standard (signal precision, calibration curve misfit and the uncertainty of the reference value). Additional uncertainties are propagated to the $^{176}Hf/^{176}Lu$ ratios from (1) the laser-induced elemental fractionation correction to the OD306 apatite standard and (2) the common Hf correction, where relevant. Resulting 2σ uncertainties for the single-grain dates are significant and are directly correlated with (1) the concentration of Lu and (2) the ingrowth time for radiogenic Hf (i.e. the Lu–Hf age) (Figure 4). Apatites with low Lu concentrations (<3 ppm) cannot be accurately dated with the current in situ Lu–Hf method, regardless of their age. Similarly, young (~0.5 Ga) apatites with Lu concentrations between 5 and 10 ppm can produce single-grain uncertainties in excess of 40%. Nonetheless, we demonstrate that for typical >1.5Ga felsic grains with Lu concentrations >10 ppm and $^{176}Hf/^{177}Hf$ ratios >20, robust in situ single grain apatite Lu–Hf dates (at 67 μm spot size) can be obtained with 2σ uncertainties <10% (Figure 4).

7 | DISCUSSION AND CONCLUSIONS

The results from this study suggest that a significant proportion (~75%) of apatites in sample AKX14-31 record U–Pb isotopic open system behaviour, induced by metamorphism. The timing of metamorphism cannot be accurately determined with the presented dataset and the U–Pb dates for those grains are geologically meaningless.

However, the corresponding Lu–Hf ages produce a ~1.8 Ga age peak that correlates with the timing of voluminous granite emplacement following the assembly of the Siberian Craton (~1.86–1.87 Ga; Donskaya et al., 2014; Gladkochub et al., 2009; Rosen, 2003; Turkina et al., 2006). The abundance of ~1.5–1.8 Ga mafic detritus in AKX14-19 is enigmatic. To the best of our knowledge, late Palaeoproterozoic–Mesoproterozoic mafic rocks are not preserved in the Biryusa uplift. However, other basement uplifts of the Siberian Craton (Anabar, Baikal and Aldan-Stanovoi uplifts) record ~1.8–1.25 Ga mafic rocks (Ernst et al., 2016), suggesting a significant amount of late Palaeoproterozoic–Mesoproterozoic mafic rocks might be currently buried by cover sequences. The late Cryogenian–early Palaeozoic detritus can be correlated with source terranes in the Yenisey ridge, Tuva-Mongolia and the Altai-Sayan foldbelt, to the south of the study area (Glorie et al., 2014; Priyatkina et al., 2018; Romanov et al., 2021).

In summary, the analysed samples for this study demonstrate the power of the method to (1) resolve the primary apatite ages for metamorphic detrital grains and (2) ensure confidence that U–Pb dates for mafic grains reflect primary ages. When the apatite Lu–Hf method, coupled with trace element data, is used in concert with apatite and zircon U–Pb geochronology, additional provenance information can be obtained, especially when fingerprinting metamorphic detritus. Given the rapidity and ease of data collection and the increasing availability of mass spectrometers fitter with reaction-cell technology, the laser-ablation-based apatite Lu–Hf method could become a routine tool for provenance research.

ORCID

Stijn Glorie https://orcid.org/0000-0002-3107-9028
Jack Gillespie https://orcid.org/0000-0002-3061-6223
Alexander Simpson https://orcid.org/0000-0001-6029-0116
Sarah Gilbert https://orcid.org/0000-0003-3259-7983
Andrei Khudoley https://orcid.org/0000-0003-3177-9734
Nadezhda Priyatkina https://orcid.org/0000-0002-0368-3105
Martin Hand https://orcid.org/0000-0003-3743-9706
Christopher L. Kirkland https://orcid.org/0000-0003-3367-8961

REFERENCES

Barfod, G. H., Krogstad, E. J., Frei, R., & Albarède, F. (2005). Lu-hf and PbSL geochronology of apatites from Proterozoic terranes: A first look at Lu-Hf isotopic closure in metamorphic apatite. *Geochimica et Cosmochimica Acta*, 69(7), 1847–1859. https://doi.org/10.1016/j.gca.2004.09.014

Barfod, G. H., Otero, O., & Albarède, F. (2003). Phosphate Lu-Hf geochronology. *Chemical Geology*, 200(3), 241–253. https://doi.org/10.1016/S0009-2541(03)00202-X

Belousova, E. A., Griffin, W. L., O'Reilly, S. Y., & Fisher, N. I. (2002). Igneous zircon: Trace element composition as an indicator of source rock type. *Contributions to Mineralogy and Petrology*, 143(5), 602–622. https://doi.org/10.1007/s00410-002-0364-7

Buslov, M. M., Geng, H., Travin, A. V., Otgonbaatar, D., Kulikova, A. V., Ming, C., Glorie, S., Semakov, N. N., Rubanova, E. S., Abildaeva, M. A., Voitishek, E. E., & Trofimova, D. A. (2013). Tectonics and geodynamics of Gorny Altai and adjacent structures of the Altai–Sayan folded area. *Russian Geology and Geophysics*, 54(10), 1250–1271. https://doi.org/10.1016/j.rgg.2013.09.009

Cawood, P. A., Hawkesworth, C. J., & Dhuime, B. (2012). Detrital zircon record and tectonic setting. *Geology*, 40(10), 875–878. https://doi.org/10.1130/G32945.1

Chew, D., O'Sullivan, G., Caracciolo, L., Mark, C., & Tyrrell, S. (2020). Sourcing the sand: Accessory mineral fertility, analytical and other biases in detrital U-Pb provenance analysis. *Earth-Science Reviews*, 202, 103093. https://doi.org/10.1016/j.earscirev.2020.103093

Chew, D. M., Petrus, J. A., & Kamber, B. S. (2014). U-Pb LA-ICPMS dating using accessory mineral standards with variable common Pb. *Chemical Geology*, 363, 185–199. https://doi.org/10.1016/j.chemgeo.2013.11.006

Chew, D. M., & Spikings, R. A. (2015). Geochronology and thermochronology using apatite: Time and temperature. *Lower Crust to Surface. Elements*, 11(3), 189–194. https://doi.org/10.2113/gselements.11.3.189

Donskaya, T. V., Gladkochub, D. P., Mazukabzov, A. M., & Wingate, M. T. D. (2014). Early Proterozoic postcollisional granitoids of the Biryusa block of the Siberian craton. *Russian Geology and Geophysics*, 55(7), 812–823. https://doi.org/10.1016/j.rgg.2014.06.002

Ernst, R. E., Okrugin, A. V., Veselovskiy, R. V., Kamo, S. L., Hamilton, M. A., Pavlov, V., Soderlund, U., Chamberlain, K. R., & Rogers, C. (2016). The 1501 Ma Kuonamka large igneous province of northern Siberia: U–Pb geochronology, geochemistry, and links with coeval magmatism on other crustal blocks. *Russian Geology and Geophysics*, 57(5), 653–671. https://doi.org/10.1016/j.rgg.2016.01.015

Fedo, C. M., Sircombe, K. N., & Rainbird, R. H. (2003). Detrital zircon analysis of the sedimentary record. *Reviews in Mineralogy and Geochemistry*, 53(1), 277–303. https://doi.org/10.2113/0530277

Galimova, T. F., Andrushenko, S. V., & Andreev, R. Y. (2000). *Geology map of Russia, scale 1/200 000, east-Sayan series, sheet N-47-II*. VSEGEI (in Russian).

Gilbert, S. E., & Glorie, S. (2020). Removal of hg interferences for common Pb correction when dating apatite and titanite by LA-ICP-MS/MS. *Journal of Analytical Atomic Spectrometry*, 35(7), 1472–1481. https://doi.org/10.1039/D0JA00224K

Gillespie, J., Glorie, S., Khudoley, A., & Collins, A. S. (2018). Detrital apatite U-Pb and trace element analysis as a provenance tool: Insights from the Yenisey ridge (Siberia). *Lithos*, 314, 140–155. https://doi.org/10.1015/j.lithos.2018.05.026

Gladkochub, D. P., Donskaya, T. V., Reddy, S. M., Poller, U., Bayanova, T. B., Mazukabzov, A. M., Dril, S., Todt, W., & Pisarevsky, S. A. (2009). Palaeoproterozoic to Eoarchaean crustal growth in southern Siberia: A Nd-isotope synthesis. *Geological Society, London, Special Publications*, 323(1), 127–143. https://doi.org/10.1144/sp323.6

Glorie, S., De Grave, J., Buslov, M. M., Zhimulev, F. I., Izmer, A., Vandoorne, W., Ryabinin, A., Van den haute, P., Vanhaecke, F., & Elburg, M. A. (2011). Formation and Palaeozoic evolution of the Gorny-Altai–Altai-Mongolia suture zone (South Siberia): Zircon U/Pb constraints on the igneous record. *Gondwana Research*, 20(2–3), 465–484. https://doi.org/10.1016/j.gr.2011.03.003

Glorie, S., De Grave, J., Buslov, M. M., Zhimulev, F. I., & Safonova, I. Y. (2014). Detrital zircon provenance of early Palaeozoic sediments at the southwestern margin of the Siberian Craton: Insights from U–Pb geochronology. *Journal of Asian Earth Sciences*, 82(Supplement C), 115–123. https://doi.org/10.1016/j.jseaes.2013.12.007

Glorie, S., Jepson, G., Konopelko, D., Mirkamalov, R., Meeuws, F., Gilbert, S., Gillespie, J., Collins, A. S., Xiao, W., Dewaele, S., & De Grave, J. (2019). Thermochronological and geochemical footprints of post-orogenic fluid alteration recorded in apatite: Implications for mineralisation in the Uzbek Tian Shan. *Gondwana Research*, 71, 1–15. https://doi.org/10.1016/j.gr.2019.01.011

Harlov, D. E. (2015). Apatite: A fingerprint for metasomatic processes. *Elements*, 11(3), 171–176. https://doi.org/10.2113/gselements.11.3.171

Henrichs, I. A., Cheve, D. M., O'Sullivan, G. J., Mark, C., McKenna, C., & Guyett, P. (2019). Trace element (Mn-Sr-Y-Th-REE) and U-Pb isotope systematics of Metapelitic apatite during progressive greenschist- to amphibolite-facies Barrovian metamorphism. *Geochemistry Geophysics Geosystems*, 20(8), 4103–4129. https://doi.org/10.1029/2019gc008359

Henrichs, I. A., O'Sullivan, G., Chew, D. M., Mark, C., Babechuk, M. G., McKenna, C., & Emo, R. (2018). The trace element and U-Pb systematics of metamorphic apatite. *Chemical Geology*, 483, 218–238. https://doi.org/10.1016/j.chemgeo.2017.12.031

Jennings, E. S., Marschall, H. R., Hawkesworth, C. J., & Storey, C. D. (2011). Characterization of magma from inclusions in zircon: Apatite and biotite work well, feldspar less so. *Geology*, 39(9), 863–866. https://doi.org/10.1130/G32037.1

Kirkland, C. L., Hollis, J., Danisik, M., Petersen, J., Evans, N. J., & McDonald, B. J. (2017). Apatite and titanite from the Karrat group, Greenland; implications for charting the thermal evolution of crust from the U-Pb geochronology of common Pb bearing phases. *Precambrian Research*, 300, 107–120. https://doi.org/10.1016/j.precamres.2017.07.033

Kirkland, C. L., Yakymchuk, C., Szilas, K., Evans, N., Hollis, J., McDonald, B., & Gardiner, N. J. (2018). Apatite: A U-Pb thermochronometer or

geochronometer? *Lithos*, *318*, 143–157. https://doi.org/10.1016/j.lithos.2018.08.007

Kochnev, B. B., & Karlova, G. A. (2010). New data on biostratigraphy of the Vendian Nemakit-Daldynian stage in the southern Siberian platform. *Stratigraphy and Geological Correlation*, *18*(5), 492–504. https://doi.org/10.1134/s0869593810050035

Letnikova, E. F., Kuznetsov, A. B., Vishnevskaya, I. A., Veshcheva, S. V., Proshenkin, A. I., & Geng, H. (2013). The Vendian passive continental margin in the southern Siberian Craton: geochemical and isotopic (Sr, Sm–Nd) evidence and U–Pb dating of detrital zircons by the LA-ICP-MS method. *Russian Geology and Geophysics*, *54*(10), 1177–1194. https://doi.org/10.1016/j.rgg.2013.09.004

Metelkin, D. V., Blagovidov, V. V., & Kazansky, A. Y. (2010). The history of the Karagas supergroup evolution in the Biryusa region: Synthesis of paleomagnetic and sedimentological data. *Russian Geology and Geophysics*, *51*(8), 868–884. https://doi.org/10.1016/j.rgg.2010.07.005

Norris, A. & Danyushevsky, L. (2018). Towards estimating the complete uncertainty budget of quantified results measured by LA-ICP-MS. *Goldschmidt Abstracts*, *1894*.

O'Sullivan, G., Chew, D., Kenny, G., Henrichs, I., & Mulligan, D. (2020). The trace element composition of apatite and its application to detrital provenance studies. *Earth-Science Reviews*, *201*, ARTN 103044. https://doi.org/10.1016/j.earscirev.2019.103044

O'Sullivan, G. J., Chew, D. M., Morton, A. C., Mark, C., & Henrichs, I. A. (2018). An integrated apatite geochronology and geochemistry tool for sedimentary provenance analysis. *Geochemistry Geophysics Geosystems*, *19*(4), 1309–1326. https://doi.org/10.1002/2017gc007343

Pisarevsky, S. A., & Natapov, L. M. (2003). Siberia and Rodinia. *Tectonophysics*, *375*(1), 221–245. https://doi.org/10.1016/j.tecto.2003.06.001

Priyatkina, N., Collins, W. J., Khudoley, A. K., Letnikova, E. F., & Huang, H.-Q. (2018). The Neoproterozoic evolution of the western Siberian craton margin: U-Pb-Hf isotopic records of detrital zircons from the Yenisey ridge and the Prisayan uplift. *Precambrian Research*, *305*, 197–217. https://doi.org/10.1016/j.precamres.2017.12.014

Roberts, N. M. W., Rasbury, E. T., Parrish, R. R., Smith, C. J., Horstwood, M. S. A., & Condon, D. J. (2017). A calcite reference material for LA-ICP-MS U-Pb geochronology. *Geochemistry, Geophysics, Geosystems*, *18*(7), 2807–2814. https://doi.org/10.1002/2016GC006784

Romanov, M., Sovetov, J. K., Vernikovsky, V. A., Rosenbaum, G., Wilde, S. A., Vernikovskaya, A. E., Matushkin, N. Y., & Kadilnikov, P. I. (2021). Late Neoproterozoic evolution of the southwestern margin of the Siberian craton: Evidence from sedimentology, geochronology and detrital zircon analysis. *International Geology Review*, *63*(13), 1658–1681. https://doi.org/10.1080/00206814.2020.1790044

Rosen, O. (2003). The Siberian craton: Tectonic zonation and stages of evolution. *Geotectonics*, *37*(3), 175–192.

Scherer, E., Münker, C., & Mezger, K. (2001). Calibration of the lutetium-hafnium clock. *Science*, *293*(5530), 683–687. https://doi.org/10.1126/science.1061372

Simpson, A., Gilbert, S., Tamblyn, R., Hand, M., Spandler, C., Gillespie, J., Nixon, A., & Glorie, S. (2021). In-situ LuHf geochronology of garnet, apatite and xenotime by LA ICP MS/MS. *Chemical Geology*, *577*, 120299. https://doi.org/10.1016/j.chemgeo.2021.120299

Stacey, J. S., & Kramers, J. D. (1975). Approximation of terrestrial Lead isotope evolution by a 2-stage model. *Earth and Planetary Science Letters*, *26*(2), 207–221. https://doi.org/10.1016/0012-821x(75)90088-6

Thompson, J., Meffre, S., Maas, R., Kamenetsky, V., Kamenetsky, M., Goemann, K., Ehrig, K., & Danyushevsky, L. (2016). Matrix effects in Pb/U measurements during LA-ICP-MS analysis of the mineral apatite. *Journal of Analytical Atomic Spectrometry*, *31*(6), 1206–1215. https://doi.org/10.1039/C6JA00048G

Turkina, O. M., Nozhkin, A. D., & Bayanova, T. B. (2006). Sources and formation conditions of early Proterozoic granitoids from the southwestern margin of the Siberian craton. *Petrology*, *14*(3), 262–283. https://doi.org/10.1134/s0869591106030040

Vermeesch, P. (2018). IsoplotR: A free and open toolbox for geochronology. *Geoscience Frontiers*, *9*(5), 1479–1493. https://doi.org/10.1016/j.gsf.2018.04.001

SUPPORTING INFORMATION

Additional supporting information may be found in the online version of the article at the publisher's website.